1R.5

MM-WAVE RADAR STRUCTURE AND MICROPHYSICAL CHARACTERISTICS OF A MIXED PHASE ALTOCUMULUS CLOUD ON 2 NOVEMBER 2001

Lawrence D. Carey[1*], Larry R. Belcher[2], J. Adam Kankiewicz[3] and Thomas H. Vonder Haar[3]

[1] Department of Atmospheric Sciences, Texas A&M University

[2] Sci. Sys. & Appl. Inc and NASA/GSFC

[3] Cooperative Institute for Research in the Atmosphere (CIRA), Colorado State University

1. INTRODUCTION

Altocumulus and altostratus clouds cover 22% of the earth (Warren et al., 1988a,b) and in turn, influence the earth's albedo and climate. Yet these mixed phase clouds have been studied far less than boundary layer or cirrus clouds. Since they rarely produce precipitation or severe weather, mid-level mixed phase clouds are the "forgotten clouds" in atmospheric science. Efforts aimed at a better understanding of cloud morphology, microphysics, and lifecycle serve to improve our ability to model and forecast these clouds, which can also impact military and civilian aviation. Satellite missions (e.g., CLOUDSAT; Stephens et al. 2002) that seek to estimate cloud properties on a global scale will benefit from knowledge of the horizontal and vertical distribution of ice and liquid water in mixed-phase clouds.

The ninth Complex Layered-Cloud Experiment (CLEX-9), conducted over western Nebraska from 8 October to 4 November 2001 provided in-situ microphysical and radar measurements of mid-level clouds from the University of Wyoming King Air research aircraft (UWKA). The 95-GHz Wyoming Cloud Radar (WCR) was deployed on the UWKA providing highly resolved radar reflectivity observations. The UWKA also measured in-cloud thermodynamic state and microphysical parameters including cloud liquid water (LWC) and ice water contents (IWC) from a suite of microphysical probes (e.g., PMS 2D-C, 2D-P, and Gerber PVM). Several surface-based instruments, including supplementary radiosonde launches, a dual-frequency radiometer, and a micropulse lidar, were located at the North Platte, Nebraska Regional Airport (LBF), providing supplementary information regarding the structure, microphysics, and environmental characteristics of the mixed phase clouds. Integration of the in-situ, airborne radar, and surface data provides the opportunity to investigate cloud morphology and the microphysical characteristics of the mixed phase clouds sampled during CLEX-9.

* *Corresponding author address*: Dr. Larry Carey, Dept. Atmospheric Sciences, Texas A&M University, College Station Texas 77843-3150; larry_carey@tamu.edu

The UWKA flew on 8 mission days during the CLEX-9 campaign. Radar and in-situ data were collected from numerous mid-level clouds using several sampling techniques (e.g., straight/level flight legs, straight-line ascents, and Lagrangian spirals) during each sortie. This paper specifically investigates the microphysical characteristics and radar structure of a dissipating mixed-phase altocumulus cloud on 2 November 2001 during CLEX-9 during a three hour period beginning shortly after sunrise. In-situ microphysical, mm-wave radar, and surface based observations are compared and contrasted at the early, mid, and dissipating phases of the observed life cycle.

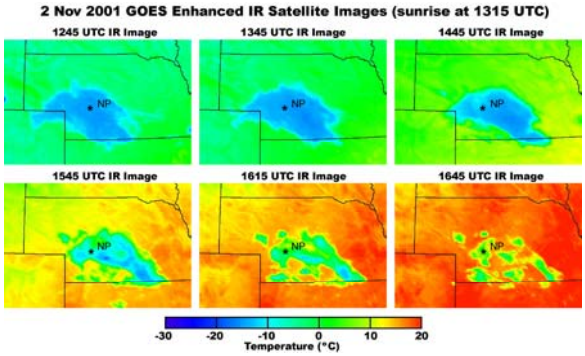

Figure 1. GOES enhanced infrared (IR) satellite imagery over North Plate (NP), Nebraska on 2 November 2001 from 30 minutes after sunrise (1245 UTC) to near dissipation of the altocumulus cloud shield at 1645 UTC.

2. OBSERVATIONS AND DISCUSSION

The altocumulus stratiformis (ACSF) cloud field over North Platte on 2 November 2001 was at its peak areal extent and minimum cloud top IR temperature (i.e., maximum cloud top height) around sunrise and slowly dissipated over the next three to four hours of the morning (Fig. 1).

The CSU micropulse lidar, which was located at the LBF, recorded a peak cloud top height of about 4.9 km mean seal level (all heights hereafter MSL) at about sunrise (1216 UTC) (Fig. 2). After sunrise, the peak cloud top height decreased for about 45 minutes and

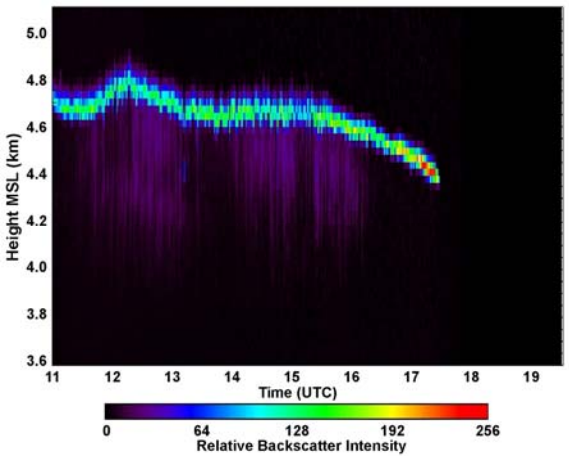

Figure 2. Time (UTC) vs. height (km, MSL) evolution of the CSU micropulse lidar relative backscatter intensity associated with an ACSF cloud over LBF from 11-18 UTC on 2 November 2001.

then stabilized at about 4.8 km until 1545 UTC when it began to decrease more rapidly until the cloud was no longer detectable over LBF by about 1730 UTC. As was confirmed with UWKA in-situ probe data (not shown), the lidar data in Fig. 2 suggest that the cloud top (where T_{top} = -12.5°C) was dominated by supercooled cloud liquid water in the upper 100-200 m (i.e., narrow layer of higher lidar intensity) of the cloud and several hundred meters (300-600 m) of precipitating ice virga below (i.e., thick region of reduced intensity). Interestingly, the ACSF cloud contained supercooled cloud water during its entire lifecycle, even up to the time of cloud dissipation, but contained ice virga primarily during the early-to-mature phase.

Figs. 3a-b show the vertically pointing WCR reflectivity factor (Z, dBZ) data taken during five-minute horizontal flight legs through the base of the virga shaft at three distinct periods during the lifecycle of the ACSF cloud shield: 1) early (1315-1320 UTC), 2) mature (1435-1440 UTC), and 3) dissipating (1600-1605 UTC). The evolution of the radar reflectivity structure in the vertical paints a fairly similar picture as the lidar data above. The cloud top was highest (4.9-5.1 km) and the cloud depth was largest (500-600km) during the early-to-mature phase of the ACSF cloud shield (Figs. 3a,b). The radar reflectivity factor reached its peak intensity (5-10 dBZ) within the individual generating cells of the ACSF cloud shield during the mature phase (Fig. 3b). By 1600 UTC, the radar detectable cloud top had decreased by about 300 m, the cloud thickness by about the same amount, since the base of the virga shaft was fairly steady while the cloud top lowered, and the peak reflectivity factor decreased dramatically to only -5 to -10 dBZ. (cf. Figs. 3b,c).

The microphysical characteristics of the liquid phase near cloud top during the early (1305-1310 UTC), mature (1417-1422 UTC), and dissipating (1550-1555 UTC) phases of the ACSF cloud shield are presented in Figs. 4a-c and summarized in Tables 1-3.

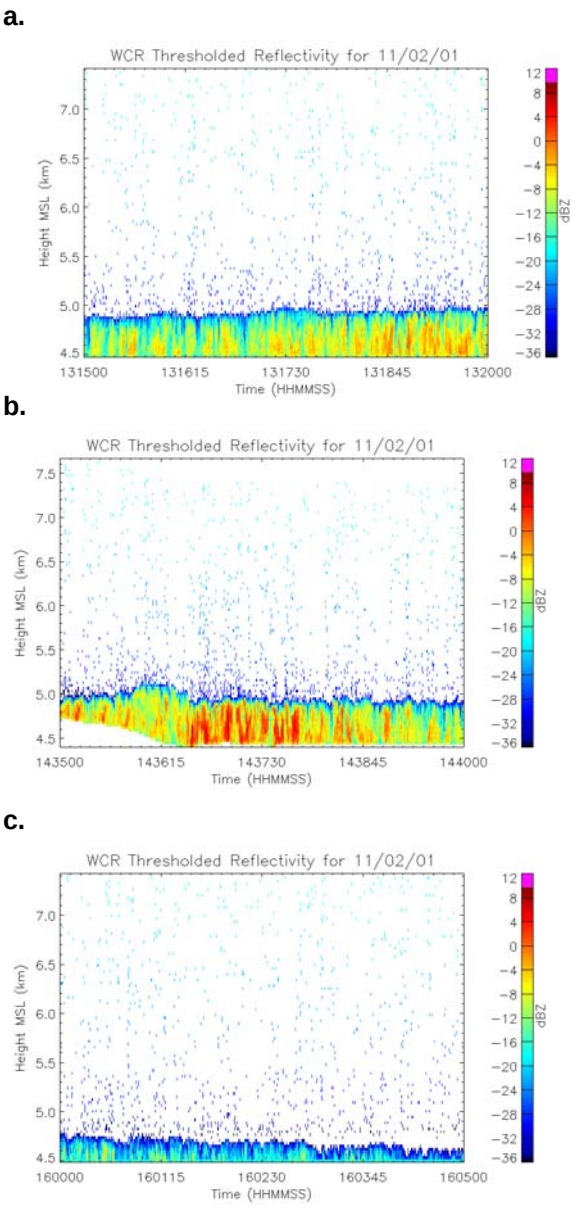

Figure 3. Vertically pointing WCR reflectivity factor (Z, dBZ) data taken during straight and level flight legs over LBF near the bottom of the virga shaft at a) early (1315-1320 UTC), b) mature (1435-1440 UTC), and c) dissipating (1600-1605 UTC) phases of the ACSF cloud shield. Since the WYKA traveled at about 100 m s^{-1}, the five minute period represents a 30 km flight leg.

As expected, the supercooled LWC at cloud top decreased from the early to the dissipating phase of the ACSF cloud shield (Fig. 4a). The mode (peak) of the supercooled LWC decreased from 0.22 (0.27) g m^{-3} to 0.14 (0.21) g m^{-3} from the early to mature phases. Although the peak supercooled LWC was much less during the dissipating phase (0.11 g m^{-3}), it is interesting to note that there was still measurable cloud LWC at this time.

a.

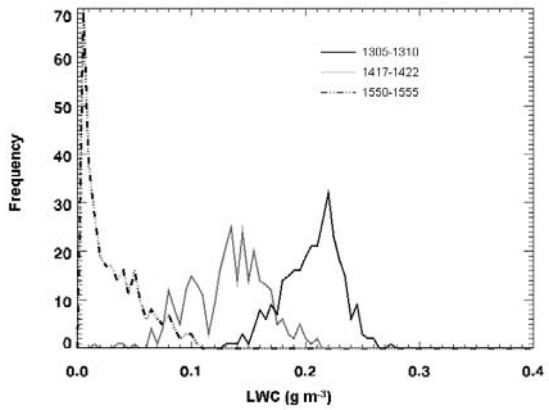

b.

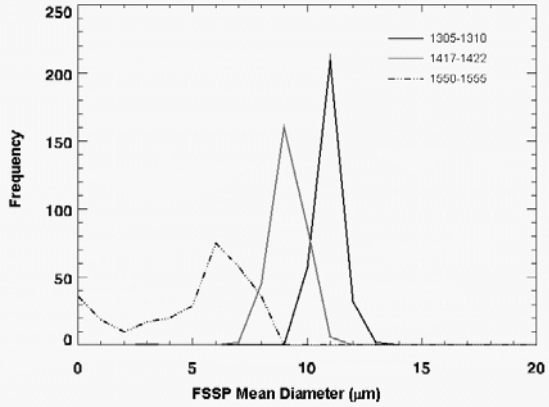

c.

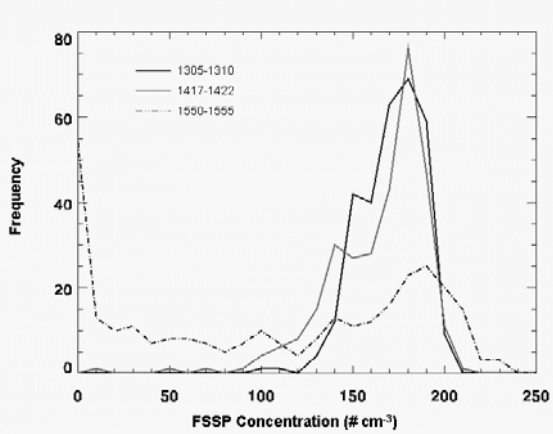

Figure 4. Frequency histograms of a) Gerber PVM liquid water content (g m^{-3}), b) FSSP mean diameter (μm), and c) FSSP total concentration (cm^{-3}) within supercooled cloud liquid water on 2 November at early (1305-1310 UTC), mature (1417-1422 UTC), and dissipating (1550-1555 UTC) phases in the ACSF cloud lifecycle during straight/level legs near cloud top.

Table 1. Gerber PVM liquid water content (LWC, g m^{-3}) statistics during the early (1305-1310 UTC), mature (1417-1422 UTC, and dissipating (1550-1555 UTC) phases near cloud top.

Gerber PVM LWC statistics	*1305-1310*	*1417-1422*	*1550-1555*
Max	0.277	0.214	0.106
Mean	0.208	0.134	0.032
Median	0.213	0.137	0.024
σ	0.025	0.033	0.025

Table 2. FSSP mean diameter (μm) statistics during the early (1305-1310 UTC), mature (1417-1422 UTC, and dissipating (1550-1555 UTC) phases near cloud top.

FSSP Mean Diameter	*1305-1310*	*1417-1422*	*1550-1555*
Max	13.13	11.73	8.92
Mean	11.47	9.67	5.32
Median	11.5	9.79	6.37
σ	0.5	0.79	2.7

Table 3. FSSP total droplet concentration (cm^{-3}) statistics during the early (1305-1310 UTC), mature (1417-1422 UTC, and dissipating (1550-1555 UTC) phases near cloud top.

FSSP Conc. Stats	*1305-1310*	*1417-1422*	*1550-1555*
Max	210	214	236
Mean	176	169	112
Median	179	177	123
σ	16	26	79

Table 4. 2D-C derived ice water content (IWC, g m^{-3}) statistics during the early (1305-1310 UTC), mature (1417-1422 UTC, and dissipating (1550-1555 UTC) phases near cloud top.

2D-C IWC Statistics	*1315-1325*	*1400-1410*	*1555-1605*
Max	0.00616	0.03053	0.00085
Mean	0.00151	0.00550	0.00017
Median	0.00108	0.00328	0.00013
σ	0.00137	0.00645	0.00017

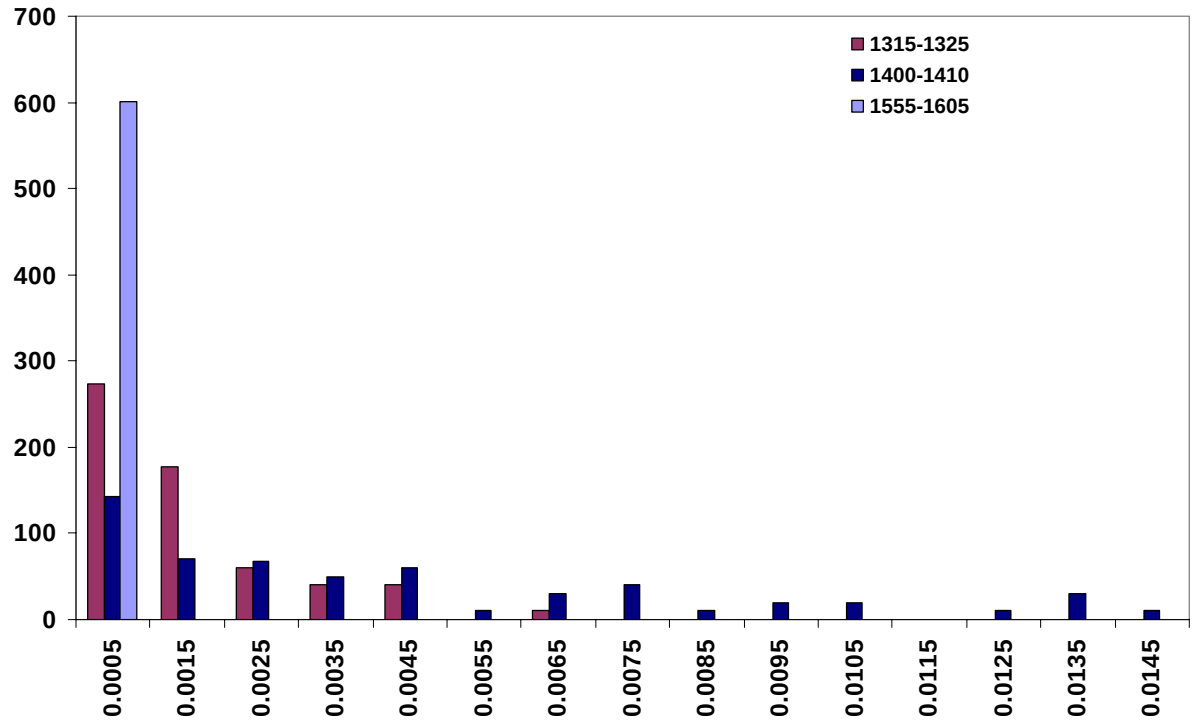

Figure 5. Histograms of IWC from 2D-C (using Mitchell et al. 1990 mass vs. diameter relationship) during 2 November 2001 at early (1315-1325 UTC, mature (1400-1410 UTC0, and dissipating (1555-1605 UTC) phases in the ACSF cloud lifecycle during straight/level legs within the 4.4 to 4.5 km altitude window for each time. Histograms constructed using 0.001 g m^{-3} bins at each time.

As presented in Fig. 4b, the Forward Scattering Spectrometer Probe (FSSP) mean diameter at cloud top shows a gradual decrease in cloud droplet modal size from about 11 μm at the early stage, to 9 μm at the mature stage, to 6 μm at the dissipating stage. The FSSP total concentration of cloud droplets near cloud top did not change significantly from the early to mature phases but decreased noticeably by the dissipating phase (Fig. 4c). Nonetheless, there were still measurable sizes and concentrations of cloud droplets as seen by the FSSP near cloud top at the dissipating stage despite some obvious signs of ice contamination at this stage.

The frequency histogram of 2D-C derived ice water content (IWC) in Fig. 5 demonstrates that the IWC peaked during the mature phase, which is consistent with the radar reflectivity data presented in Fig. 3. Interestingly, the IWC decreased even more rapidly than the LWC from the mature to dissipating phases, which is also consistent with the dramatic (15 dBZ) decrease in the overall WCR reflectivity factors. A summary of the IWC statistics by stage can be found in Table 4. 2D-C image data (not shown) indicates that pristine plate-like (stellar and dendritic) crystals were the dominate ice habit, as expected. Inspection of the 2D-C image data also confirmed that pristine ice crystal sizes and aggregation of these crystals peaked during the mature phase, resulting in the maximum IWC and radar reflectivity factor shown earlier.

Apparently, the ice factory slowed down and the larger ice crystals and aggregates precipitated out of the ACSF cloud shield between the mature to dissipating phases, despite the remaining presence of some supercooled water at the dissipating phase. This apparent “de-glaciation” is somewhat at odds with the classic conceptual model of the dissipation of mixed-phase AC clouds by glaciation (Hobbs and Rangno 1985) and will be investigated further.

3. REFERENCES

Hobbs, P. V., and A. L. Rangno, 1985: Ice particle concentrations in clouds. *J. Atmos. Sci.*, **42**, 2523-2549.

Mitchell, D. L., R. Zhang, and R. Pitter, 1990: Mass-dimensional relationships for ice particles and the influence of riming on snowfall rates. *J. Appl. Meteor.,* **29,** 153–163.